



# Benchmark *N*-glycoproteomics study of common differential tissue and serum *N*-glycoproteins of patients with hepatocellular carcinoma

Ming Bi<sup>a,1</sup>, Ke Gao<sup>b,1</sup>, Bing Bai<sup>c,\*</sup>, Zhixin Tian<sup>a,\*\*</sup>

<sup>a</sup> School of Chemical Science & Engineering, Tongji University, Shanghai, 200092, China

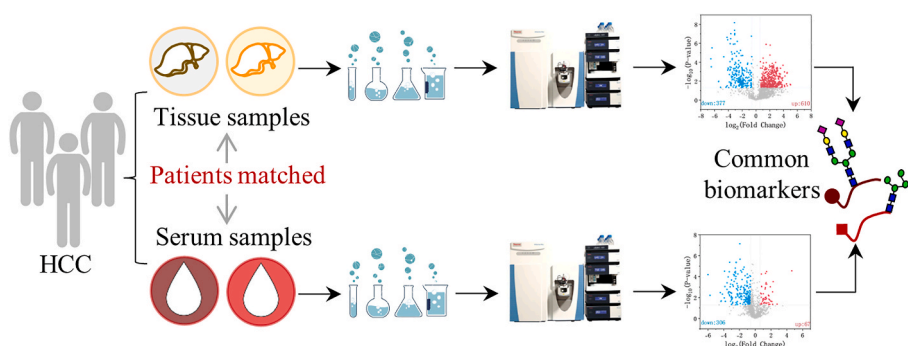
<sup>b</sup> Department of Liver Surgery and Transplantation, and Key Laboratory of Carcinogenesis and Cancer Invasion (Ministry of Education), Liver Cancer Institute, Zhongshan Hospital, Fudan University, Shanghai 200032, China

<sup>c</sup> Department of Laboratory Medicine, Center of precision Medicine, Nanjing Drum Tower Hospital, the Affiliated Hospital of Nanjing University Medical School, Nanjing, Jiangsu, 210008, China

## HIGHLIGHTS

- Comparative *N*-glycoproteomics study of matched tissue and serum from HCC patients.
- 344 and 127 differentially expressed *N*-glycoproteins were quantified at the intact *N*-glycopeptide level from the tissue and serum samples, and 29 are common.
- Subcellular localization confirmed the tissue origin of the 29 common *N*-glycoproteins.

## GRAPHICAL ABSTRACT



## ARTICLE INFO

Handling Editor: Dr. L. Liang

### Keywords:

HCC  
tissue  
Serum  
*N*-glycoprotein biomarker  
LC-MS/MS  
GPSeeker

## ABSTRACT

For hepatocellular carcinoma (HCC), *N*-glycosylation has been proved to be widely involved in various aspects of the disease, including development, metastasis, subtyping, diagnosis and prognosis. The common practice is to discover biomarkers in situ of cancer occurrence (i.e., cancer vs. adjacent tissues) yet to clinically monitor in sera because of non-invasiveness. This study benchmarks *N*-glycoproteomics characterization of common differential tissue and serum *N*-glycoproteins of patients with HCC. Differential *N*-glycosylation in matched tissue and serum samples from the same patients were quantitatively characterized at the intact *N*-glycopeptide molecular level, and 29 common *N*-glycoproteins were found. Subcellular localization analysis was carried out to confirm the tissue originality. Secreted *N*-glycoprotein APOH was up-regulated, and transmembrane and intracellular *N*-glycoproteins including OSMR, GAT2, CSF-1 and MAGI3 were down-regulated.

\* Corresponding author.

\*\* Corresponding author.

E-mail addresses: [bing.bai@nju.edu.cn](mailto:bing.bai@nju.edu.cn) (B. Bai), [zhixintian@tongji.edu.cn](mailto:zhixintian@tongji.edu.cn) (Z. Tian).

<sup>1</sup> Equal contribution.

## 1. Introduction

Hepatocellular carcinoma (HCC), ranking as the sixth most prevalent cancer and third leading cause of cancer deaths worldwide, is attributed to various etiologies including virus infection, alcohol abuse, high calorie diets and irregular rest [1,2]. In the study of the underlying mechanism of tumor formation and diagnostic biomarkers, proteomics and glycoproteomics has merged as meaningful research hotspots [3,4]. The combination of alpha-fetoprotein (AFP-L3) and des-gamma-carboxy prothrombin (DCP) is the diagnostic biomarker for HCC approved by Food and Drug Administration (FDA) [5]. Compared to proteomics, glycoproteomics has greater precision in clinical applications with the glycosite and glycan signatures [6]. Liu et al. [7] applied lectin arrays to serum glycoproteins from HCC and cirrhosis patients and founded that fucosylation were significantly increased in HCC patients. With the development of molecularly imprinted polymers (MIPs), terminal sialylation was founded highly correlated with HCC [8]. For haptoglobin (Hp), *N*-glycan N5H6F1S3 at *N*-glycosite N184 and N241 showed good performance for distinguishing HCC from cirrhosis [9]. Alpha-1-antitrypsin (A1AT) modified with N4H5S2 at Asn271 expressed discriminate in early HCC [10].

Sera, being secreted by organs and circulated in the whole organism, provide a micro window for observation and assessment of the overall state of the body. From the proteome point, the proteins in plasma are primarily secreted by liver and intestine, subsequently filtered by kidney [11]. The plasma proteome is deeply influenced by the physiological state and in turn serving as a reflection of health [12]. Proteins temporarily present in plasma or serum participating in a myriad of biological functions including immune responses, antigen-antibody binding reaction, enzymatic reaction and so on. Tissues, especially carcinoma ones, release proteins into plasma. Consequently, sera specimens are suitable for disease diagnostics due to their minimal invasive nature.

Proteins derived from plasma or serum exhibited a high degree of glycosylation. *N*-glycan also reflects a change of diseases or cancers [13]. The extent of shared glycoproteins between tissues and sera remains largely unknown. Zhang et al. [14] employed mass spectrometry (MS) to detect *N*-glycopeptides from cells, tissues and plasma, revealing a notable overlap among different sample types, which confirmed that MS is capable of detecting tissue-derived glycoproteins in plasma. In the study of 13 colorectal cancer patients, Coura and coworkers identified 26 *N*-glycans differentially expressed in plasma compared to healthy plasma and 11 *N*-glycans altered in tumor tissue compared to adjacent tissue in which 8 *N*-glycans were shared in the two samples but without consistently expression [15]. With *N*-glycomics study of a tissue discovery cohort, a tissue validation cohort and one independent serum cohort consisting of patients with intrahepatic cholangiocarcinoma (iCCA), HCC, or benign chronic liver disease, Shaaron and coworkers validated 12 *N*-glycans altered consistently in both tissue and serum; fucosylated bisected and triantennary structures discriminated patient iCCA from non-iCCA [16].

This study reported benchmark *N*-glycoproteomics study of common differential tissue and serum *N*-glycoproteins of patients with HCC at the intact *N*-glycopeptide molecular level.

## 2. Experimental

**Materials and Reagents.** SDS, Tris, urea, ammonium bicarbonate (ABC) and BCA Protein Assay Kit were purchased from Sagon Biotech (Shanghai, China). Dithiothreitol (DTT), iodoacetamide (IAA), acetonitrile (ACN), trifluoroacetic acid (TFA), formic acid (FA) and sodium cyanoborohydride, acetaldehyde-<sup>13</sup>C<sub>2</sub> (99 atom % <sup>13</sup>C) were purchased from Sigma-Aldrich (St. Louis, USA). Sequencing grade modified trypsin was bought from Promega (Madison, USA). Acetaldehyde solution (40 % in H<sub>2</sub>O) and ammonium hydroxide solution were from General Reagent (Shanghai, China). Ultrapure water was produced onsite with a

Millipore Simplicity System (Billerica, MA, USA).

**Sample preparation of intact *N*-glycopeptides from tissues and sera.** Both tissue and serum specimens from three HBV-related HCC patients were from Zhongshan Hospital, and the study was approved by the ethic committee (B2019-100R) (detailed in Table S1). The workflow of sample preparation is showed in Fig. S1. Tissue samples were stored in −80 °C until homogenized in SDS/TRIS (HCl) solution at a ratio of 1:20 (v/v) along with a cocktail and shaking for 30 min. The resulting mixture was then centrifugated at 14,000 rpm for 30 min, and the supernatant was collected and added to ice-cold acetone for precipitation in −20 °C for 3 h. The protein pellets, from centrifugation at 10,000 g for 10 min, were then redissolved in 8 M urea and diluted with 50 mM ABC until the urea concentration was reduced to below 1 M. 5 mL of venous blood were drawn from each individual (drawn before any treatments and surgery), placed in room temperature for 1 h until coagulated, and serum was recovered by centrifugation at 3000 rpm for 10 min and stored in aliquots at −80 °C until further use. 15 µL package serum were denaturized by 8 M urea and diluted with 50 mM ABC to the urea concentration below 1 M.

After denaturation protein concentrations were detected by BCA Protein Assay Kit. 500 µg proteins from tumor and adjacent samples and proteins from 15 µL serum from patient and healthy volunteers were continued to next procedures. Proteins were reduced with 200 mM (final concentration) DTT at 55 °C for 20 min, followed by alkylation with final concentration of 200 mM IAA in the dark for 30 min. Subsequently, a final concentration of 200 mM DTT was added to the protein solution to react with any remaining IAA. The protein solution was mixed with trypsin (1:50, w/w) in approximately 5 mL 50 mM ABC solution and incubated 16 h with gentle shaking at 37 °C.

The digested peptides were desalted using C18 (25 mg, 15 µm, Jupiter, Phenomenex) solid phase extraction (SPE) columns. After equilibrated with 80 % ACN containing 0.1 % TFA and subsequently 0.1 % TFA, the desalting SPE column were loaded in digestion solution for 5 times for sufficient binding. After 8 times wash by 0.1 % TFA, peptides were eluted by 50 % ACN containing 0.1 % TFA and 80 % ACN containing 5 % TFA. The eluants were combined, dried in a Speed-Vac (Thermo Fisher Scientific, USA), and redissolved in 100 µL 80 % ACN containing 5 % TFA.

Peptides were labeled with stable isotopic diethylation (SIDE) as previously reported [17]. Briefly, peptides re-suspended in 100 µL TFE, and 100 µL 20 % acetaldehyde (for healthy specimen) or acetaldehyde-<sup>13</sup>C<sub>2</sub> (for disease specimen) was added. Subsequently, 100 µL freshly prepared 600 mM NaBH<sub>3</sub>CN was added and incubated at 37 °C for 1 h, and the reaction was quenched with incubation with 100 µL 10 % (v/v) NH<sub>4</sub>OH followed by addition of 75 µL 5 % (v/v) FA. Heavy labeled and light labeled peptides were mixed together at 1:1 ratio (w/w) and dried in the Speed-Vac.

After desalting by C18 SPE columns, intact *N*-glycopeptides were enriched from labeled peptides by ZIC-HILIC (15 mg, 5 µm, SeQuant, Merck) SPE columns. The column was equilibrated with 0.1 % TFA and subsequently 80 % ACN containing 5 % TFA. After loading, 800 µL 80 % ACN containing 5 % TFA was applied to wash non-glycosylated peptides; 300 µL 0.1 % TFA and 100 µL 50 mM ABC were used to elute glycopeptides and the eluants were combined and dried in the Speed-Vac. Dried labeled intact *N*-glycopeptides were dissolved in 30 µL H<sub>2</sub>O for downstream LC-MS/MS analysis.

**RPLC-MS/MS analysis of intact *N*-glycopeptides.** The experiments were performed on Dionex Ultimate 3000 RSLC coupled to nano-ESI Q Exactive MS (Thermo Fisher Scientific, San Jose, CA, USA). Chromatographic columns packed with C18 (5 µm, Jupiter, Phenomenex) were composed of trap column (5 cm long, 200 µm i.d) and analytical column (60 cm long, 75 µm i.d). Buffer A was 0.2 % FA aqueous solution, and Buffer B was 95 % ACN with 0.2 % FA. The loading and elution flow rates were 3.0 and 0.3 µL/min, respectively. The multi-step gradient settings were as follows: 2 % buffer B 20 min, 2–40 % buffer B 190 min, 40–95 % buffer B 10 min, 95 % buffer B 10 min, 95–2 % buffer B 10 min,

2 % buffer B 10 min.

The spray voltage, ion transfer tube temperature and S-lens RF level were 2.8 kV, 250 °C and 50 %, respectively. MS spectra were acquired with the parameters of  $m/z$  700–2000, mass resolution 70,000, automatic gain control (AGC) target 1e6, maximum injection time 200 ms. MS/MS spectra were acquired in the DDA mode for Top20 ions with mass resolution 17,500, AGC target 5e5, maximum injection time 250 ms, isolation windows 2  $m/z$ , higher energy collision dissociation with normalized collision energies of 20 %/30 %/30 % and dynamic exclusion time 20 s.

With the aforementioned LC-MS/MS settings, three technical replicates were acquired to obtain three.raw files for every paired sample.

**Identification and quantitation of intact *N*-glycopeptides.** Raw datasets were searched by intact *N*-glycopeptide search engine GPSeeker for identification and quantification. The mass level 1 parameter settings were as follows: isotopic peak  $m/z$  deviation (IPMD) 20 ppm, isotopic peak relative abundance cutoff (IPACO) 40 %, isotopic peak relative abundance deviation (IPAD) 50 %, precursor isolation window 2 Th. The

mass level 2 parameter settings were as follows: isotopic peak  $m/z$  deviation (IPMD) 20 ppm, isotopic peak relative abundance cutoff (IPACO) 40 %, isotopic peak relative abundance deviation (IPAD) 50 %. The tissue theory forward databases were constructed with 20,417 protein entries (UniProt Human database) and 75,888 *N*-glycans while the serum theory forward databases were constructed with 6191 (UniProt Human plasma database) protein entries and 75,888 *N*-glycans. Furthermore, the corresponding reversed databases were constructed with the inverted sequence of peptides and *N*-glycans each with random addition of 1–30 Da. Target and decoy GPSMs were combined and ranked by P scores; a cut-off P score is then chosen to give spectrum-level FDR ≤ 1 % and final IDs after duplicate removal.

The abundance of the paired precursor ions with light  $-CH_2CH_3$  and heavy  $-^{13}CH_2^{13}CH_3$  labels was adopted for relative quantitation. With the criteria of no less than twice observation among the three technical replicates,  $P$ -value ≤ 0.05, and fold change no less than 1.5, differentially expressed intact *N*-glycopeptides (DEGPs) were obtained.

**Function annotation of the differentially expressed intact *N*-**

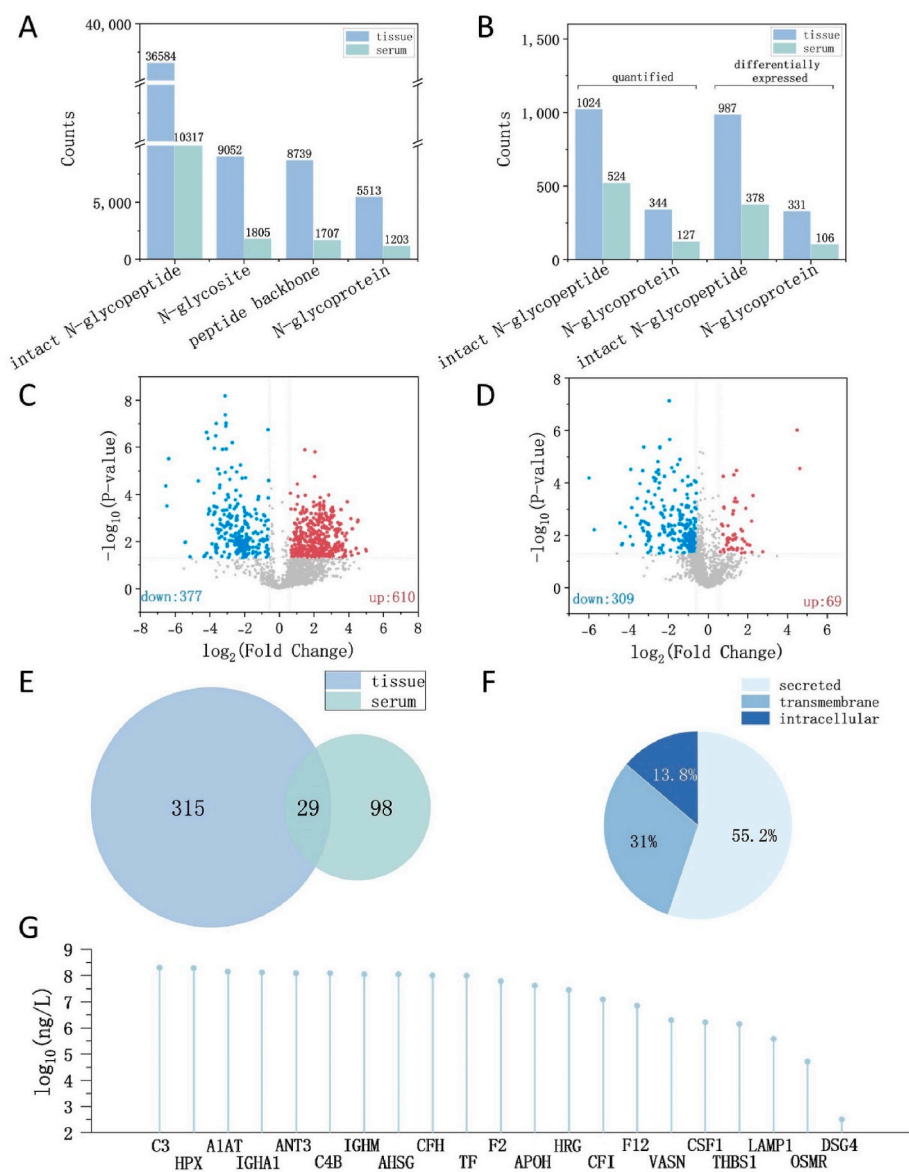


**Fig. 1.** Qualitative and quantitative *N*-glycoproteomics results in the HCC tissue and serum samples; (A) qualitative results of tissue and serum samples, (B) quantitative results of the tissue and serum samples, (C) volcano plot of the tissue samples, (D) volcano plot of the serum samples, (E) overlap of the quantitative results between the tissue and serum samples, (F) subcellular distribution of the common *N*-glycoproteins, (G) reported concentration of the common *N*-glycoproteins in PeptideAtlas.

**glycopeptides.** Included annotations are GO in the PANTHER knowledgebase (<http://pantherdb.org/>), KEGG in The Database for Annotation, Visualization and Integrated Discovery (DAVID, <https://david.nci.fcrf.gov/>) and PPI in STRING (<https://cn.string-db.org/>).

SignalP 6.0 (predicting a signal peptide), TMHMM 2.0 (predicting transmembrane (TM) regions) and SecreteomeP 2.0 (predicting non-classical secretory protein without signal peptide) were adopted for subcellular localization of secreted, transmembrane and intracellular proteins. If a protein was predicted with signal peptide and without TM regions, the protein was thought secreted; if a protein was predicted with TM regions, the protein was transmembrane protein; if a protein without signal peptides and TM regions at the meantime not belong to non-classical secretory protein, the protein was thought an intracellular protein.

### 3. Results and discussions

#### Intact *N*-glycopeptides identified and quantified in the HCC

**tissue samples.** For the analysis of HCC tumor and paracancerous tissues, in *N*-glycoproteomics 36,584 intact *N*-glycopeptides were identified, corresponding to 9052 *N*-glycosites, 8739 peptide backbones, and 5513 *N*-glycoproteins (Fig. 1A). For quantitation, in *N*-glycoproteomics 12,680 intact *N*-glycopeptides were quantified once, 2888 no less than twice, and 987 as DEGs (no less than twice,  $p\text{-value} \leq 0.05$ , fold change  $\geq 1.5$ ) including 610 up-regulated and 377 down-regulated (Fig. 1B and C); these 987 DEGs correspond to 331 *N*-glycoproteins (detailed in Supplementary Table S2).

**Intact *N*-glycopeptides identified and quantified in the HCC serum samples.** For the analysis of HCC serum vs. the healthy control, in *N*-glycoproteomics 10,317 intact *N*-glycopeptides were identified corresponding to 1805 *N*-glycosites, 1707 peptide backbones and 1,203 *N*-glycoproteins (Fig. 1A). For quantitation, in *N*-glycoproteomics 5388 intact *N*-glycopeptides were quantified at least once. 1890 at least twice, and 378 as DEGs (no less than twice,  $p\text{-value} \leq 0.05$ , fold change  $\geq 1.5$ ) including 69 up-regulated and 309 down-regulated (Fig. 1B and D). These 378 DEGs correspond to 106 *N*-glycoproteins (detailed in

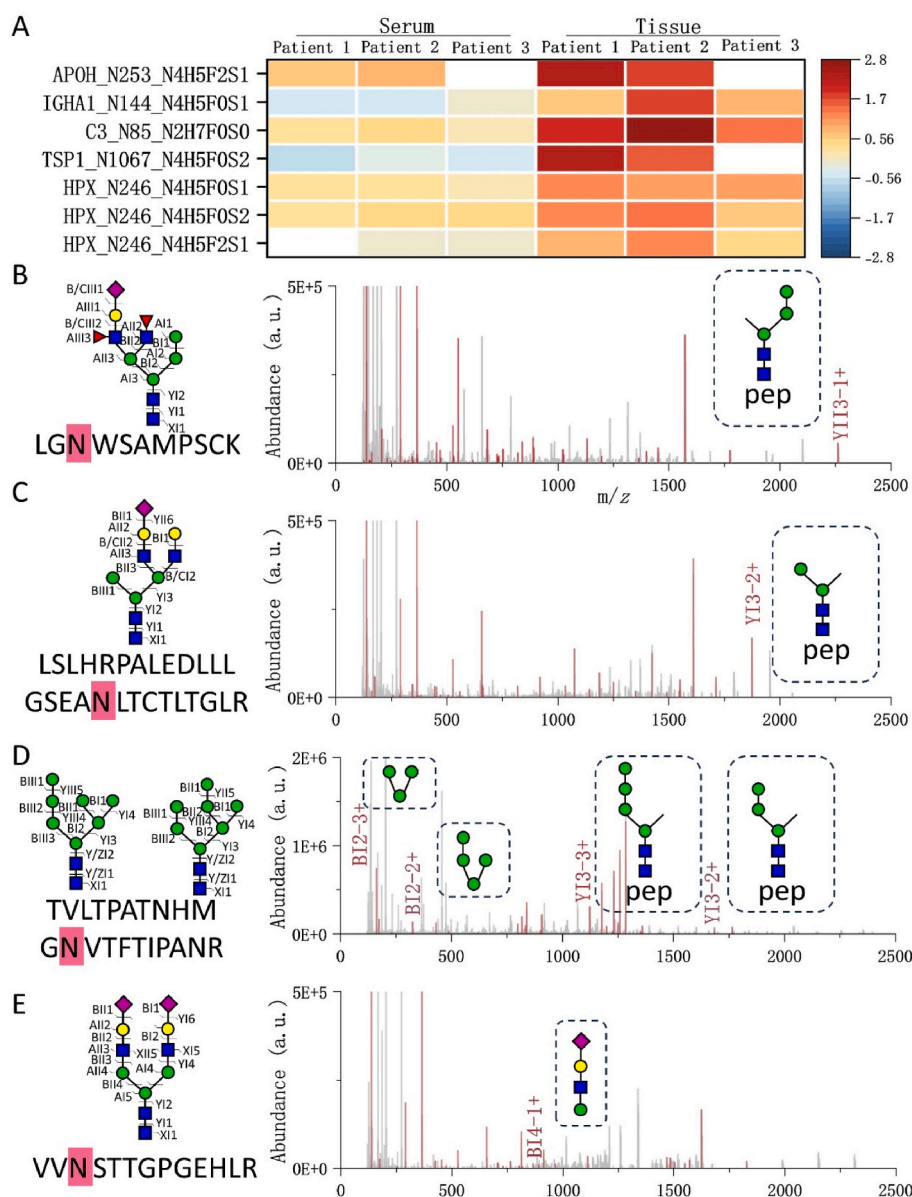


**Fig. 2.** Intact *N*-glycopeptides from secreted *N*-glycoproteins quantitative in both the HCC serums and tissue samples. (A) heatmap, (B–E) graphical fragmentation map and annotated structure-diagnostic ions in the MS/MS spectra for intact *N*-glycopeptides identified from apolipoprotein H (APOH, N253), immunoglobulin heavy constant alpha 1 (IGHA1, N144), complement C3 (C3, N85) and thrombospondin 1 (TSP1, N1067).



### Supplementary Table S2).

In reference to the protein concentrations in Human Protein Atlas [18], the absolute concentrations of the *N*-glycoproteins qualified and quantified in the HCC sera were queried (Fig. S1). Among the *N*-glycoproteomics results, the concentration of the 449 identified *N*-glycoproteins range from 4.2 ng/L to 440 mg/L and among the 254 quantified *N*-glycoproteins, ceruloplasmin (CP) has the highest concentration of 440 mg/L and cadherin 4 (CDH4) has the lowest concentration of 19 ng/L.

**Commonly *N*-glycoproteins quantified in both the tissue and serum samples.** Among the *N*-glycoproteins corresponding to the DEGs from the tissue and serum samples, 29 are common (Fig. 1E) including 16 secreted, 9 transmembrane, and 4 intracellular (Fig. 1F). The subcellular localization confirms these *N*-glycoproteins are originally tissue proteins and released into sera, and thus can serve as putative serum for HCC in this study. 86.7 % of these 29 *N*-glycoproteins have MS-estimated seral concentration [18] with a range of 320 ng/L to 200 mg/L (Fig. 1G).

**Putative serum biomarkers from secreted *N*-glycoproteins.** Most commonly altered *N*-glycoproteins in both tissue and serum are liver secreted proteins indicating their potential as promising HCC diagnostic biomarkers. Seven intact *N*-glycopeptides were quantified in both tissue and serum samples corresponding to five *N*-glycoproteins including beta-2-glycoprotein 1 (APOH, P02749), immunoglobulin heavy constant alpha 1 (IGHA1, P01876), complement C3 (C3, P01024), thrombospondin-1 (TSP1, P07996) and hemopexin (HPX, P02790) (Fig. 2A).

For APOH, from *N*-glycosite N253 intact *N*-glycopeptide LGNWSAMPSCCK with *N*-glycan monosaccharide composition N4H5F2S1 and linkage structure (01Y41Y41 M(31 M(21Y(31F)41L32S) 41Y31F)61M61 M) was quantified both in tissue and serum samples with the fold change of  $4.20 \pm 0.90$  (p-value = 0.01) and  $1.79 \pm 0.12$  (p-value = 0.009) (Fig. 2B). The structure-diagnostic ion YII3 (*m/z* 2264.03, 1+) from the *N*-glycan moiety confirmed the unique tri-antennary structure with two branch fucoses and a sialic acid; the composition N4H5F2S1 has 13 putative sequence structures in the theoretical database adopted in this study. APOH is a liver-secreted glycoprotein abundant in plasma. With MS identification, MRM verification and immunohistochemistry validation in tissue, Yang et al. [19] proposed aberrant APOH peptides EHSSLAFWK and ATVVYQGER as putative biomarkers. The tri-antennary glycoform with fucose in APOH was also previously confirmed in HCC sera [20]. Up-regulation of APOH is associated with the acute phase of HBV infection and its interaction with hepatitis B surface antigen (HBsAg) can initiate endoplasmic reticulum (ER) stress [21]. APOH has been proven to play a mediating role in HBV infection in cell lines [22].

For IgA, intact *N*-glycopeptide LSLHRPALEDLLGSEANLTCTLTGLR with *N*-glycan structure 01Y41Y41 M(31 M)61 M(21Y41L32S)61Y41L was identified from *N*-glycosites N144; and the *N*-glycan structure was verified with structure-diagnostic fragment ions of YI3 (*m/z* 1876.46, 2+) (Fig. 2C). IgA has been recognized for its diagnostic potential in early HCC detection and glycosylated IgA has been observed in the development of liver cancer [23,24]. IgA contributes to aggravating inflammation or dismantling antitumor immunity in human diseased liver [25] and apolipoprotein B mRNA editing enzyme catalytic subunit 3F (APOBEC3F) may active intestinal immune network for IgA production signaling pathway, leading to malignant biological behaviors of HCC cells [26]. Up-regulation of mono-sialylated *N*-glycan was also previously reported in an *N*-glycomics study of liver cirrhosis patients serum [27].

For C3, high-mannose *N*-glycan with monosaccharide composition of N2H7F0S0 at *N*-glycosite N85 was upregulated ( $4.67 \pm 1.79$ , p-value = 0.001) in the tissue samples whereas unchanged ( $1.22 \pm 0.12$ , p-value = 0.03) in the serum samples. For N2H7F0S0, two sequence structures 01Y41Y41 M(31M21 M)61 M(31M21 M)61 M and 01Y41Y41 M(31M21M21 M)61 M(31 M)61 M were observed and confirmed with

structure-diagnostic ions of YI3 (*m/z* 1685.81, 2+ and *m/z* 1124.21, 3+) (Fig. 2D). Chang et al. [28] also reported the correlation of this up-regulated *N*-glycosylation with the tumor grade in HCC, cholangiocarcinoma (CCA), and cHCC-CCA (combined HCC and CCA). C3 can induce T-cell apoptosis and reduce the inhibition of CD4<sup>+</sup> and CD8<sup>+</sup> T-cell proliferation, decrease expressions of CD11c, CD80, CD86, and MHCII, while increase CD274 expression resulting in dominant immunosuppression and tumor progression [29]. In PPI network, 15 out of common 29 glycoproteins showed a tight correlation with each other and C3 was a core protein in the 15 glycoproteins (Figure S2 A). Furthermore, complement and coagulation cascades were significantly enriched in KEGG pathway analysis and C3 is a key protein in the complement and coagulation cascades which are tightly related with HCC [30–32] (Figure S2 B). Zhang et al. [33] statistically analyzed the gene expression of 220 HBV-related HCC patients and found that the complement and coagulation cascades pathway was significantly enriched in differentially expressed genes. Coagulation and complement cascades are key components among immunological networks in liver and influence tumor immune microenvironment deeply in HCC [34,35].

For TSP1, bi-antennary sialylated *N*-glycan (N4H5F0S2) at *N*-glycosite N1067 was slightly down-regulated ( $0.64 \pm 0.11$ ) in the serum sample whereas up-regulated ( $4.04 \pm 1.45$ ) in the tissue samples (Fig. 2E). TSP1 is highly expressed in HCC patient correlated with tumor progression and is a putative postoperative biomarker [36,37]. Several factors such as viral infection, alcohol consumption and obesity can lead to increase of TSP1 in liver contributing to liver fibrosis or non-alcoholic fatty liver disease (NAFLD) [38]. TSP1 converts latent transforming growth factor-beta1 (TGF-beta 1) complexes into their biologically active form to inhibit liver regeneration [39]. The signal transduction of CD74 and TSP1 would increase tumor growth [40].

For HPX, in the serum samples three down-regulated intact *N*-glycopeptides were quantified (Fig. 3A and B); on *N*-glycosite N187 and N453 the same *N*-glycan structure was down-regulated with fold changes of  $0.55 \pm 0.07$  (p-value = 0.02) and  $0.48 \pm 0.03$  (p-value = 0.005) (Fig. 3A). In the tissue sample, uniform up-regulation was observed; for example, on *N*-glycosite N246 *N*-glycan 01Y41Y41 M(31 M(21Y(31F)41L32S)41Y31F)61M61 M has a fold change of  $1.76 \pm 0.45$  (p-value = 0.02) (Fig. 3B). On *N*-glycosite N246 *N*-glycan structures 01Y41Y41 M(31 M)61 M(21Y41L32S)61Y41L, 01Y41Y41 M(31M41Y41L32S)61M61Y41L32S and 01Y41Y41 M(31 M(21Y(31F) 41L32S)41Y31F)61M61 M were commonly quantified (Fig. 3C); up-regulation in the tissue samples and no apparent change in the serum samples were observed. Kobayashi and coworkers [41] purified fucosylated HPX from HCC patients serum and tissues by lectin ELISA and found that the level of fucosylated HPX was no significant different in cancer tissue and non-cancerous tissue but performed differently in serum samples. Fucosylated HPX had an AUROC of 0.9515 with an optimal sensitivity of 92 % and a specificity of 92 % diagnostic ability through over 300 HCC patient serum proved by targeted lectin extraction [42]. Benicky et al. verified that outer arm fucosylated bi- and tri-antennary HPX at *N*-glycosite N187 was related to liver disease [43]. HPX, as a secreted protein with 190 mg/L concentration in serum, has emerged as a potential candidate biomarker for diagnosing HCC. Researches employing data independent acquisition (DIA) MS method and high-sample-throughput multiple reaction monitoring mass spectrometric (HST-MRM-MS) methods have demonstrated the utility of HPX in distinguishing HCC patient serum [44,45]. HPX functions to protect body against free heme-induced oxidative damage and has anti-inflammatory property [46,47]. In case of acute-on-chronic liver failure in HBV patients, HPX would decreased and was related with inflammatory response [48].

**Putative serum biomarkers from transmembrane *N*-glycoproteins.** Compared with secreted *N*-glycoproteins, transmembrane *N*-glycoproteins including Oncostatin-M-specific receptor subunit beta (OSMR, Q99650), sodium- and chloride-dependent GABA transporter 2 (GAT2, Q9NSD5) and macrophage colony-stimulating factor 1(CSF-1,

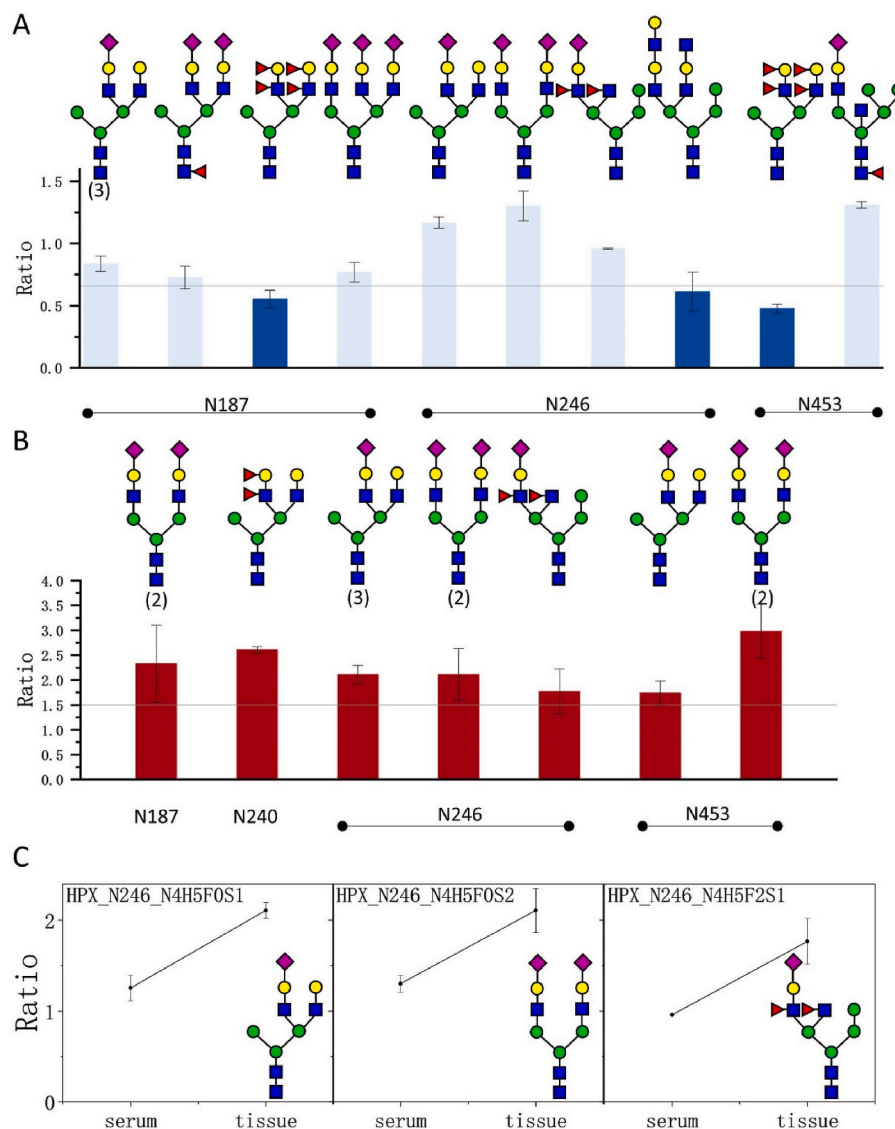


**Fig. 3.** Site- and structure-specific *N*-glycosylation expression of intact *N*-glycopeptides quantified for hemopexin (HPX) in the HCC sera (A) and tissues (B) and both sera and tissues (C).

P09603) were all down-regulated in both the tissue and the serum samples (Fig. 4).

For **OSMR**, on *N*-glycosite N163 *N*-glycan N4H5F0S2 was found significantly down-regulated in the tissue ( $0.13 \pm 0.05$ ,  $p$ -value = 0.02) and the sera ( $0.12 \pm 0.005$ ,  $p$ -value = 0.0005) (Fig. 4A). The structure-diagnostic ions YI3-2+ ( $m/z$  1264.10 and  $m/z$  1592.21) confirmed the bi- and tri-antennary structures (Fig. 4B and C). OSMR is one of the receptors of oncostatin M (OSM) transducing OSM signals corresponding to gene expression and cell proliferation [49]. The overexpressed OSM acted as a profibrogenic factor by directly stimulating migration of hepatic myofibroblasts [50]; whereas OSMR activated Janus kinase 2 (JAK2)/STAT3 in the liver and protected against obesity-induced hepatic insulin resistance, inflammatory responses, which was validated in hepatic tissues in both human and mouse models [51]. Hematopoiesis of the OSMR gene knock-out mice were founded compromised [52]. The deficiency or down-expression of OSMR had bad effect of liver and in our results, down-regulated intact *N*-glycopeptide of OSMR obviously existed in HCC patients.

For **GAT2**, the intact *N*-glycopeptide TNGSLNGTSE-NATSPVIEFWER\_N3H3F0S0 exhibited down-regulation in both the tissue ( $0.17 \pm 0.04$ ,  $p$ -value = 0.0002) and the serum ( $0.20 \pm 0.02$ ,  $p$ -

value = 0.002) samples. The *N*-glycan structure was identified by structure-diagnostic ions YI3 ( $m/z$  1066.16, 3+) (Fig. 4D and E). GAT2 is a protein mostly expressed in the plasma membranes of periportal hepatocytes [53]. The deletion of GAT2 gene led to 50 % reduction of taurine level in liver [53], and the serum level of taurine has been determined by LC-MS to be lower in the advanced HCC stage relative to the early stage, which is associated with the development and progression of HCC; and thus taurine serves as a metabolic biomarker [54].

For **CSF-1**, on *N*-glycosite N381 down-regulation of *N*-glycan N4H5F2S0 were observed in both the tissue and the serum samples (Fig. 4G) with fold changes of  $0.10 \pm 0.07$  ( $p$ -value = 0.04) and  $0.11 \pm 0.05$  ( $p$ -value = 0.02) (Fig. 4F). CSF-1 is a hematopoietic growth factor produced by various cells and the concentration in plasma is about 10 ng/mL [55,56]. CSF-1 is crucial in regulating immunity and modulating the abundance of specific intestinal microorganisms and their metabolites to prevent HCC as validated in murine model [57]. High expression of CSF-1 was widely observed in advanced cancer cells [58,59]. The high expression of CSF-1 was proved to influencing oncogenesis and immunity in vitro experiments and CSF-1 could be a putative therapeutic and prognostic target for HCC [60].

OSMR, CSF-1 and TSP-1 were all enriched in the PI3K-AKT pathway

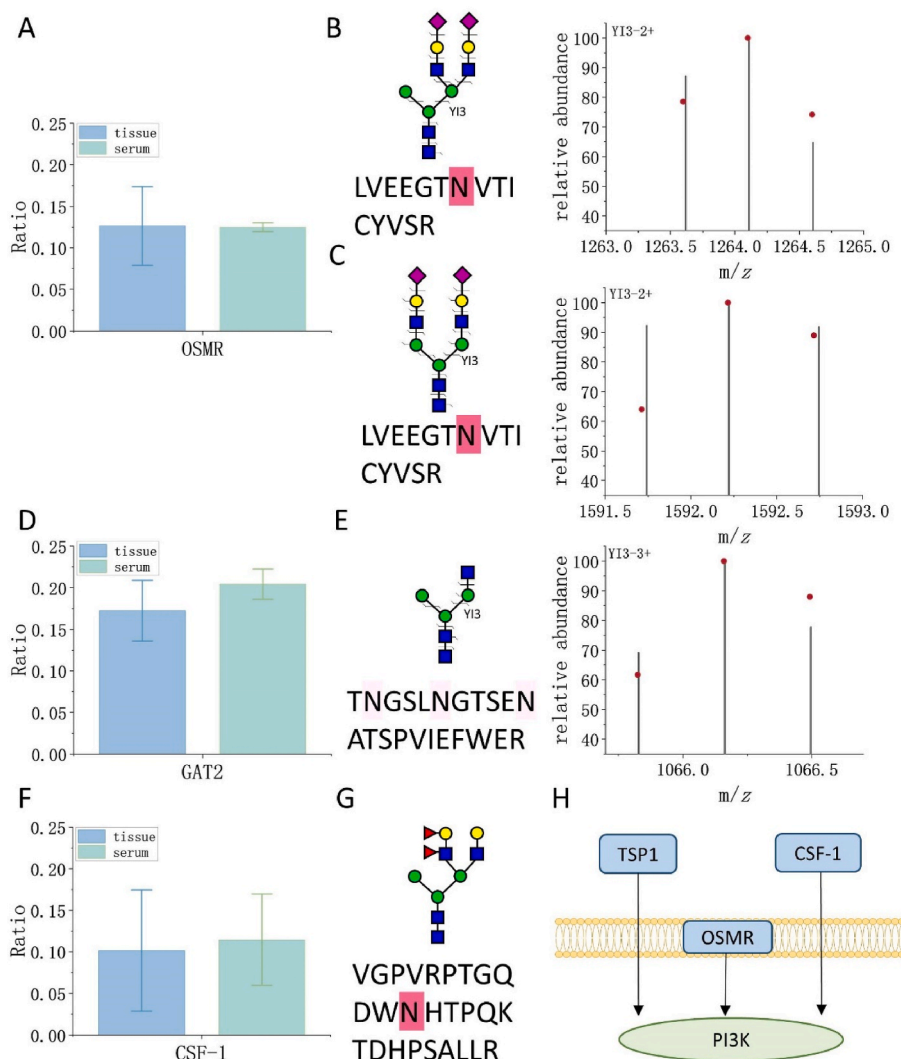


**Fig. 4.** Intact *N*-glycopeptides from transmembrane *N*-glycoproteins quantitative in both the HCC serum and tissue samples. Fold change, graphical fragmentation map and isotopic envelope fingerprinting maps of structure-diagnostic fragment ions of oncostatin M receptor (OSMR, A/B/C), solute carrier family 6 member 13 (S6A13, D/E) and colony stimulating factor 1 (CSF-1, F/G), (H) PI3K activation pathway.

which increases tumor cells proliferation [61] (Fig. 4H). Knock-down of OSMR by RNA interference led to strong activation of the PI3K/Akt pathways in the murine model [62]. Wang et al. [63] proved that long intergenic non-protein coding RNA 520 (LINC00520) could regulate OSMR to promote the progression of acute kidney injury (AKI) via the PI3K/AKT signaling pathway. CSF-1 induced phosphorylation of Y721 (pY721) in association with the p85 regulatory subunit of phosphoinositide 3-kinase (PI3K) [64,65].

#### Putative serum biomarkers from Intracellular *N*-glycoproteins.

For membrane-associated guanylate kinase, WW and PDZ domain-containing protein 3 (MAGI3, Q5TCQ9), significant down-regulation of EAIN<sub>249</sub>GSGNAENRER\_N4H5F1S1 was observed in both the tissue ( $0.12 \pm 0.02$ ,  $p$ -value = 0.002) and the serum ( $0.12 \pm 0.02$ ,  $p$ -value = 0.004) samples. The structure-diagnostic ions YI3 ( $m/z$  1225.55, 2+) and YI13 ( $m/z$  1306.58, 2+) revealed two structures 01Y(61F)41Y41 M (31 M(21Y41L32S)41Y)61M61 M and 01Y(61F)41Y41 M(31 M)61 M (21Y41L32S)61Y41L (Fig. 5). MAGI3, known as an inverted membrane-associated guanylate kinase, is localized to epithelial cell tight junctions [66] and functions as a scaffolding protein at cell-cell junctions [67]. The decrease of MAGI3 was related to activation of the Wnt/ $\beta$ -catenin signaling and enhancement of cell migration and invasion in cervical cancer [68]. Additionally, MAGI3 has been identified as a direct functional target of miR-34c-3p in regulating glycolysis and oncogenic

activities in HCC, predicting poor clinical outcomes for patients [67]. The PI3K-Akt signaling pathway, enriched in tissue differentially expressed proteins according to KEGG analysis, is known to regulate glycolysis in cancer cells [69].

It should be noted that the linkage structures of *N*-glycans come from the biosynthetic rules as adopted during the construction of the theoretical *N*-glycan DB; only 48.76 % and 61.33 % monosaccharide sequence structures of the intact *N*-glycopeptide IDs in serum and tissue samples are distinguished from their isomers with structure-diagnostic fragment ions, and the underlying reasons include but not limited to absence of theoretical structure-diagnostic fragment ion(s), limited fragmentation efficiency, low abundance in the sample, enormous sequence isomers. In addition, the sample size of this study is very limited, and further study of larger sample size will consolidate the practice of discovery of *N*-glycoprotein biomarkers in tissues whereas clinic non-invasive diagnosis in sera.

#### 4. Conclusions

Following the practice of biomarker discovery in tissues while validation in sera, common putative tissue and serum *N*-glycoprotein biomarkers of hepatocellular carcinoma were characterized with *N*-glycoproteomics study of the matched tissue and serum samples from

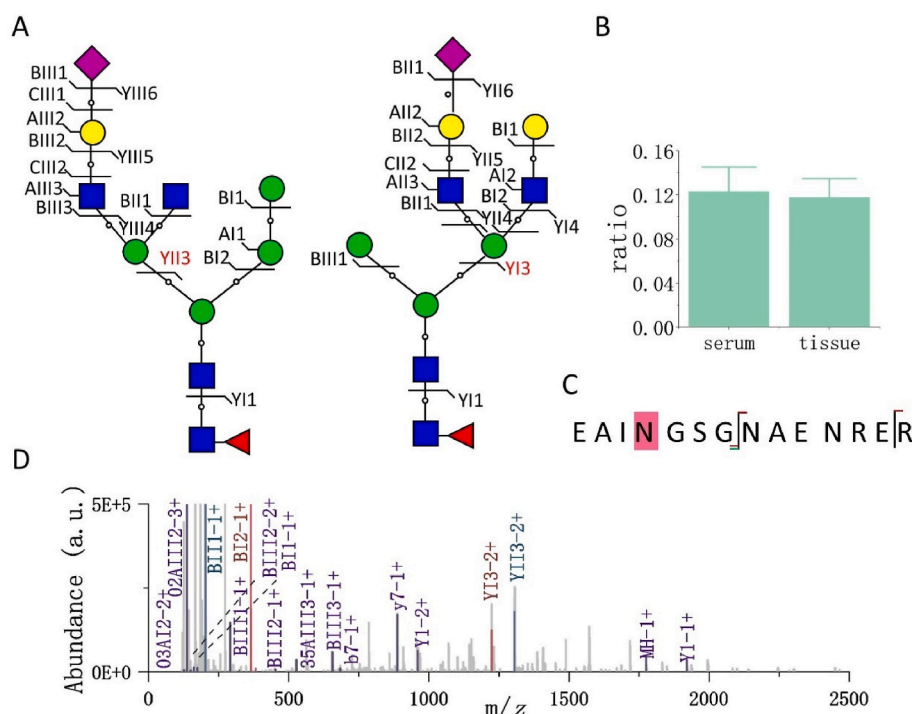


**Fig. 5.** The graphical fragmentation map (A), differential expression ratios (B), peptide backbone fragmentation (C) and annotated MS/MS spectra (D) of intact *N*-glycopeptide EAINGSGNAENRER\_N4H5F1S1 identified from *N*-glycosite N249 of *N*-glycoprotein Membrane-associated guanylate kinase, WW and PDZ domain-containing protein 3 (MAGI3) in the HCC serum and tissue samples.

the same patients. 29 common putative *N*-glycoprotein biomarkers were found, including 16 secreted, 9 transmembrane, and 4 intracellular. These common intact *N*-glycopeptides of secreted *N*-glycoproteins were all upregulated in tissue samples and more prominently expressed than in serum samples. The shared intact *N*-glycopeptides of transmembrane and intracellular *N*-glycoproteins were decreased in both tissue and serum samples.

#### CRediT authorship contribution statement

**Ming Bi:** Writing – original draft, Visualization, Software, Formal analysis, Data curation. **Ke Gao:** Resources. **Bing Bai:** Conceptualization. **Zhixin Tian:** Writing – review & editing, Project administration, Funding acquisition.

#### Declaration of Competing interest

The authors declare no conflict of interest.

#### Data availability

Data will be made available on request.

#### Acknowledgements

This research was financially supported by National Science Foundation of China (22074105) and Shanghai Science and Technology Commission (14DZ2261100).

#### Appendix A. Supplementary data

Supplementary data to this article can be found online at <https://doi.org/10.1016/j.aca.2024.343066>.

#### References

- [1] N.E. Rich, Changing epidemiology of hepatocellular carcinoma within the United States and worldwide, *Surg. Oncol. Clin.* 33 (1) (2024) 1–12.
- [2] Y.K. Sim, M.C. Chong, M. Gandhi, et al., Real-world data on the diagnosis, treatment and management of hepatocellular carcinoma in the asia-pacific: the insight study, *Liver Cancer* 13 (3) (2023) 306–321.
- [3] Y. Wang, H. Chen, Protein glycosylation alterations in hepatocellular carcinoma: function and clinical implications, *Oncogene* 42 (24) (2023) 1970–1979.
- [4] M.O. Dobrica, C. Lazar, N. Branza-Nichita, *N*-glycosylation and *n*-glycan processing in hbv biology and pathogenesis, *Cells* 9 (6) (2020).
- [5] R.J. Wong, A. Ahmed, R.G. Gish, Elevated alpha-fetoprotein differential diagnosis - hepatocellular carcinoma and other disorders, *Clin. Liver Dis.* 19 (2) (2015) 309–+.
- [6] Y.Q. Zheng, K. Gao, Q. Gao, et al., Glycoproteomic contributions to hepatocellular carcinoma research: a 2023 update, *Expert Rev. Proteomics* 20 (10) (2023) 211–220.
- [7] Y.S. Liu, J.T. He, C. Li, et al., Identification and confirmation of biomarkers using an integrated platform for quantitative analysis of glycoproteins and their glycosylations, *J. Proteome Res.* 9 (2) (2010) 798–805.
- [8] P.F. Li, J.L. Pang, S.X. Xu, et al., A glycoform-resolved dual-modal ratiometric immunoassay improves the diagnostic precision for hepatocellular carcinoma, *Angewandte Chemie-International Edition* 61 (21) (2022).
- [9] J.H. Zhu, J.F. Huang, J. Zhang, et al., Glycopeptide biomarkers in serum haptoglobin for hepatocellular carcinoma detection in patients with nonalcoholic steatohepatitis, *J. Proteome Res.* 19 (8) (2020) 3452–3466.
- [10] H.D. Yin, J.H. Zhu, M.M. Wang, et al., Quantitative analysis of  $\alpha$ -1-antitrypsin glycosylation isoforms in hcc patients using lc-hcd-prm-ms, *Anal. Chem.* 92 (12) (2020) 8201–8208.
- [11] N.L. Anderson, N.G. Anderson, The human plasma proteome - history, character, and diagnostic prospects, *Mol. Cell. Proteomics* 1 (11) (2002) 845–867.
- [12] P.E. Geyer, N.A. Kulak, G. Pichler, et al., Plasma proteome profiling to assess human health and disease, *Cell Systems* 2 (3) (2016) 185–195.
- [13] M.E. Yaman, H.M. Kayili, M. Albayrak, et al., Differential *n*-glycosylation profiling of formalin-fixed paraffin-embedded (ffpe) invasive ductal carcinoma tissues using maldi-tof-ms, *Molecular Omics* 17 (3) (2021) 394–404.
- [14] H. Zhang, A.Y. Liu, P. Loriaux, et al., Mass spectrometric detection of tissue proteins in plasma, *Mol. Cell. Proteomics* 6 (1) (2007) 64–71.
- [15] M.D.A. Coura, E.A. Barbosa, G.D. Brand, et al., Identification of differential *n*-glycan compositions in the serum and tissue of colon cancer patients by mass spectrometry, *Biology-Basel* 10 (4) (2021).
- [16] S. Ochoa-Rios, C.R.K. Blaschke, M. Wang, et al., Analysis of *n*-linked glycan alterations in tissue and serum reveals promising biomarkers for intrahepatic cholangiocarcinoma, *Cancer research communications* 3 (3) (2023) 383–394.
- [17] Y. Wang, K.J. Xiao, Z.X. Tian, Quantitative *n*-glycoproteomics using stable isotopic diethyl labeling, *Talanta* 219 (2020).



- [18] T. Farrah, E.W. Deutsch, G.S. Omenn, et al., A high-confidence human plasma proteome reference set with estimated concentrations in peptideAtlas, *Mol. Cell. Proteomics* 10 (9) (2011).
- [19] W.Q. Cao, B.Y. Jiang, J.M. Huang, et al., Straightforward and highly efficient strategy for hepatocellular carcinoma glycoprotein biomarker discovery using a nonglycopeptide-based mass spectrometry pipeline, *Anal. Chem.* 91 (19) (2019) 12435–12443.
- [20] E.S. Ji, H. Hwang, G.W. Park, et al., Analysis of fucosylation in liver-secreted n-glycoproteins from human hepatocellular carcinoma plasma using liquid chromatography with tandem mass spectrometry, *Anal. Bioanal. Chem.* 408 (27) (2016) 7761–7774.
- [21] Y.M. Liu, J.L. Maiers, Y.J. Rui, et al., Apolipoprotein h drives hepatitis b surface antigen retention and endoplasmic reticulum stress during hepatitis b virus infection, *Int. J. Biochem. Cell Biol.* 131 (2021).
- [22] P.J. Gao, Y. Shi, Y.H. Gao, et al., The receptor for  $\beta_2$ gp i on membrane of hepatocellular carcinoma cell line smmc-7721 is annexin ii, *World J. Gastroenterol.* 13 (24) (2007) 3364–3368.
- [23] S. Zhang, X. Cao, C. Liu, et al., N-glycopeptide signatures of iga2 in serum from patients with hepatitis b virus-related liver diseases, *Molecular & cellular proteomics : MCP* 18 (11) (2019) 2262–2272.
- [24] T. Yang, X.Q. Lin, L.M. Zhang, et al., Integration of iga and iga autoantibodies for early diagnosis of hepatocellular carcinoma, *Clin. Chim. Acta* 523 (2021) 423–429.
- [25] P.S. Sung, D.J. Park, P.R. Roh, et al., Intrahepatic inflammatory iga<sup>+</sup>pd-1<sup>high</sup> monocytes in hepatocellular carcinoma development and immunotherapy, *Journal for Immunotherapy of Cancer* 10 (5) (2022).
- [26] Z.G. Yang, Y.Q. Tao, X. Xu, et al., Bufalin inhibits cell proliferation and migration of hepatocellular carcinoma cells via apobec3f induced intestinal immune network for iga production signaling pathway, *Biochem. Biophys. Res. Commun.* 503 (3) (2018) 2124–2131.
- [27] Y. Carré, A. Klein, P. Mathurin, et al., Changes of serum-associated fucosylated glycoproteins and changes in glycosylation of iga in human cirrhosis, *Proteomics Clin. Appl.* 3 (5) (2009) 609–622.
- [28] T.T. Chang, J.H. Cheng, H.W. Tsai, et al., Plasma proteome plus site-specific n-glycoproteins for hepatobiliary carcinomas, *Journal of Pathology Clinical Research* 5 (3) (2019) 199–212.
- [29] Y.P. Xu, Y.H. Huang, W.Q. Xu, et al., Activated hepatic stellate cells (hscs) exert immunosuppressive effects in hepatocellular carcinoma by producing complement c3, *Oncotargets Ther.* 13 (2020) 1497–1505.
- [30] W. Dong, Z.Y. Xia, Z.H. Chai, et al., Proteomic analysis of small extracellular vesicles from the plasma of patients with hepatocellular carcinoma, *World J. Surg. Oncol.* 20 (1) (2022).
- [31] J.Y. Zhang, R. Liang, J.Z. Wei, et al., Identification of candidate biomarkers in malignant ascites from patients with hepatocellular carcinoma by itraq-based quantitative proteomic analysis, *BioMed Res. Int.* 2018 (2018).
- [32] L. Li, Q.S. Lei, S.J. Zhang, et al., Screening and identification of key biomarkers in hepatocellular carcinoma: evidence from bioinformatic analysis, *Oncol. Rep.* 38 (5) (2017) 2607–2618.
- [33] Y. Zhang, X.R. Chen, Y.J. Cao, et al., C8b in complement and coagulation cascades signaling pathway is a predictor for survival in hbv-related hepatocellular carcinoma patients, *Cancer Manag. Res.* 13 (2021) 3503–3515.
- [34] A. Malik, U. Thanekar, S. Amarachintha, et al., "Complementing the complement": mechanistic insights and opportunities for therapeutics in hepatocellular carcinoma, *Front. Oncol.* 10 (2021).
- [35] Q.F. He, J. Yang, Y.H. Jin, Immune infiltration and clinical significance analyses of the coagulation-related genes in hepatocellular carcinoma, *Briefings Bioinf.* 23 (4) (2022).
- [36] R.T. Poon, K.K. Chung, S.T. Cheung, et al., Clinical significance of thrombospondin 1 expression in hepatocellular carcinoma, *Clin. Cancer Res.* 10 (12) (2004) 4150–4157.
- [37] P. Starlinger, S. Haegel, D. Wanek, et al., Plasma thrombospondin 1 as a predictor of postoperative liver dysfunction, *Br. J. Surg.* 102 (7) (2015) 826–836.
- [38] Y.Z. Li, C.P. Turpin, S.X. Wang, Role of thrombospondin 1 in liver diseases, *Hepatol. Res.* 47 (2) (2017) 186–193.
- [39] H. Hayashi, K. Sakai, H. Baba, et al., Thrombospondin-1 is a novel negative regulator of liver regeneration after partial hepatectomy through transforming growth factor-beta1 activation in mice, *Hepatology* 55 (5) (2012) 1562–1573.
- [40] D.D. Roberts, S. Kaur, D.R. Soto-Pantoja, Therapeutic targeting of the thrombospondin-1 receptor cd47 to treat liver cancer, *Journal of Cell Communication and Signaling* 9 (1) (2015) 101–102.
- [41] S. Kobayashi, K. Nouse, H. Kinugasa, et al., Clinical utility of serum fucosylated hemopexin in Japanese patients with hepatocellular carcinoma, *Hepatol. Res.* 42 (12) (2012) 1187–1195.
- [42] M.A. Comunale, M.J. Wang, J. Hafner, et al., Identification and development of fucosylated glycoproteins as biomarkers of primary hepatocellular carcinoma, *J. Proteome Res.* 8 (2) (2009) 595–602.
- [43] J. Benicky, M. Sanda, P. Pompach, et al., Quantification of fucosylated hemopexin and complement factor h in plasma of patients with liver disease, *Anal. Chem.* 86 (21) (2014) 10716–10723.
- [44] H.C. Jiang, L. Zhang, Y. Zhang, et al., Hst-mrm-ms: a novel high-sample-throughput multiple reaction monitoring mass spectrometric method for multiplex absolute quantitation of hepatocellular carcinoma serum biomarker, *J. Proteome Res.* 18 (1) (2019) 469–477.
- [45] L.P. Zhao, J.H. Shi, L. Chang, et al., Serum-derived exosomal proteins as potential candidate biomarkers for hepatocellular carcinoma, *ACS Omega* 6 (1) (2021) 827–835.
- [46] V. Hvidberg, M.B. Maniecki, C. Jacobsen, et al., Identification of the receptor scavenging hemopexin-heme complexes, *Blood* 106 (7) (2005) 2572–2579.
- [47] X.Y. Liang, T. Lin, G.J. Sun, et al., Hemopexin down-regulates lps-induced proinflammatory cytokines from macrophages, *J. Leukoc. Biol.* 86 (2) (2009) 229–235.
- [48] N. Zhou, K.F. Wang, S.H. Fang, et al., Discovery of a potential plasma protein biomarker panel for acute-on-chronic liver failure induced by hepatitis b virus, *Front. Physiol.* 8 (2017).
- [49] F. Blanchard, Y.P. Wang, E. Kinzie, et al., Oncostatin m regulates the synthesis and turnover of gp130, leukemia inhibitory factor receptor alpha, and oncostatin m receptor beta by distinct mechanisms, *J. Biol. Chem.* 276 (50) (2001) 47038–47045.
- [50] B. Foglia, S. Sutti, D. Pedicini, et al., Oncostatin m, a profibrogenic mediator overexpressed in non-alcoholic fatty liver disease, stimulates migration of hepatic myofibroblasts, *Cells* 9 (1) (2020).
- [51] P.C. Luo, P.X. Wang, Z.Z. Li, et al., Hepatic oncostatin m receptor beta regulates obesity-induced steatosis and insulin resistance, *Am. J. Pathol.* 186 (5) (2016) 1278–1292.
- [52] K. Nakamura, H. Nonaka, H. Saito, et al., Hepatocyte proliferation and tissue remodeling is impaired after liver injury in oncostatin m receptor knockout mice, *Hepatology* 39 (3) (2004) 635–644.
- [53] Y. Zhou, S. Holmseth, C.Y. Guo, et al., Deletion of the gamma-aminobutyric acid transporter 2 (gat2 and slc6a13) gene in mice leads to changes in liver and brain taurine contents, *J. Biol. Chem.* 287 (42) (2012) 35733–35746.
- [54] W.J. Wang, J.X. Lv, N. Chen, et al., Dysregulated serum metabolites in staging of hepatocellular carcinoma, *Clin. Biochem.* 61 (2018) 7–11.
- [55] I. Ushach, A. Zlotnik, Biological role of granulocyte macrophage colony-stimulating factor (gm-csf) and macrophage colony-stimulating factor (m-csf) on cells of the myeloid lineage, *J. Leukoc. Biol.* 100 (3) (2016) 481–489.
- [56] T. Okazaki, S. Ebihara, M. Asada, et al., Macrophage colony-stimulating factor improves cardiac function after ischemic injury by inducing vascular endothelial growth factor production and survival of cardiomyocytes, *Am. J. Pathol.* 171 (4) (2007) 1093–1103.
- [57] Y.N. Wu, L. Zhang, T. Chen, et al., Granulocyte-macrophage colony-stimulating factor protects mice against hepatocellular carcinoma by ameliorating intestinal dysbiosis and attenuating inflammation, *World J. Gastroenterol.* 26 (36) (2020).
- [58] X.D. Zhu, J.B. Zhang, P.Y. Zhuang, et al., High expression of macrophage colony-stimulating factor in peritumoral liver tissue is associated with poor survival after curative resection of hepatocellular carcinoma, *J. Clin. Oncol.* 26 (16) (2008) 2707–2716.
- [59] J.F. Zhou, L. Liu, X.D. Hu, et al., Matrix metalloproteinase-21 promotes metastasis via increasing the recruitment and m2 polarization of macrophages in hcc, *Cancer Sci.* 114 (2) (2023) 423–435.
- [60] T.X. Xiang, N. Cheng, B. Huang, et al., Important oncogenic and immunogenic roles of spp1 and csf1 in hepatocellular carcinoma, *Med. Oncol.* 40 (6) (2023).
- [61] M.D.A. Paskeh, F. Ghadyani, M. Hashemi, et al., Biological impact and therapeutic perspective of targeting pi3k/akt signaling in hepatocellular carcinoma: promises and challenges, *Pharmacol. Res.* 187 (2023).
- [62] J. Drechsler, J. Grötzinger, H.M. Hermanns, Characterization of the rat oncostatin m receptor complex which resembles the human, but differs from the murine cytokine receptor, *PLoS One* 7 (8) (2012).
- [63] X.H. Tian, Y.Q. Ji, Y.F. Liang, et al., Linc00520 targeting mir-27b-3p regulates *osmr* expression level to promote acute kidney injury development through the pi3k/akt signaling pathway, *J. Cell. Physiol.* 234 (8) (2019) 14221–14233.
- [64] K.A. Mouchemore, N.G. Sampaio, M.W. Murrey, et al., Specific inhibition of pi3k p110 $\delta$  inhibits csf-1-induced macrophage spreading and invasive capacity, *FEBS J.* 280 (21) (2013) 5228–5236.
- [65] N.G. Sampaio, W.F. Yu, D. Cox, et al., Phosphorylation of csf-1r y721 mediates its association with pi3k to regulate macrophage motility and enhancement of tumor cell invasion, *J. Cell Sci.* 124 (12) (2011) 2021–2031.
- [66] Y. Wu, D. Dowbenko, S. Spencer, et al., Interaction of the tumor suppressor pten/mmac with a pzd domain of magi3, a novel membrane-associated guanylate kinase, *J. Biol. Chem.* 275 (28) (2000) 21477–21485.
- [67] Q.Y. Weng, M.J. Chen, W.B. Yang, et al., Integrated analyses identify mir-34c-3p/magi3 axis for the warburg metabolism in hepatocellular carcinoma, *Faseb. J.* 34 (4) (2020) 5420–5434.
- [68] Z.L. Yang, H. Liu, R. Song, et al., Reduced magi3 level by hpv18e6 contributes to wnt/beta-catenin signaling activation and cervical cancer progression, *Fabs Open Bio* 11 (11) (2021) 3051–3062.
- [69] J. Feng, J.J. Li, L.W. Wu, et al., Emerging roles and the regulation of aerobic glycolysis in hepatocellular carcinoma, *J. Exp. Clin. Cancer Res.* 39 (1) (2020).